Contrib Mineral Petrol (2004) 148: 201–215
DOI 10.1007/s00410-004-0591-1

ORIGINAL PAPER

Etienne Médard · Max W. Schmidt · Pierre Schiano

Liquidus surfaces of ultracalcic primitive melts: formation conditions and sources

Received: 3 December 2003 / Accepted: 21 May 2004 / Published online: 14 August 2004

Abstract CaO-rich, Al_2O_3-poor ultracalcic primitive melts occur at mid-ocean-ridges, back-arc basins, ocean islands and volcanic arcs. They are subdivided into a ''nepheline-normative'' alkaline-rich, silica-poor group uniquely found in arcs and in ''hypersthene-normative'' fairly refractory melts which occur in all of the above environments. The high CaO contents (to 19.0 wt%) and CaO/Al_2O_3 ratios (to 1.8) exclude an origin from fertile lherzolites at volatile-absent conditions. Experimental investigation of the liquidus of a hypersthene-normative and a nepheline-normative ultracalcic melt results in quite distinct pressure-temperature conditions of multiple saturation: whereas the hypersthene-normative liquid saturates in olivine + clinopyroxene at 1.2 GPa and 1,410°C, this occurs at 0.2 GPa and 1,220°C for the nepheline-normative ultracalcic liquid. Our results in combination with melting experiments from the literature suggest that hypersthene-normative melts result from melting of a refractory olivine + clinopyroxene ± orthopyroxene source at elevated mantle temperatures. Contrasting, nepheline-normative ultracalcic melts form from wehrlitic cumulates in the arc crust; to account for the high alkaline and low silica contents, and the relatively low temperatures, source wehrlites must have contained amphibole.

Editorial Responsibility: V. Trommsdorff

E. Médard (✉) · P. Schiano
Laboratoire Magmas et Volcans, OPGC,
Université Blaise Pascal—CNRS, 5 rue Kessler,
63038 Clermont-Ferrand, France
E-mail: E.Medard@opgc.univ-bpclermont.fr
Tel.: +33-473-346723
Fax: +33-473-346744

M. W. Schmidt
Institut für Mineralogie und Petrographie,
ETH-Zentrum, Sonneggstrasse 5,
8092 Zürich, Switzerland

Introduction

Partial melting of lherzolites is thought to be the dominant process by which primary basaltic to picritic magmas form (e.g., Jaques and Green 1980; BVSP 1981). Studies of mantle xenoliths and orogenic peridotites as well as isotope modelling have revealed that at least the uppermost part of the mantle contains modally variable lherzolites to harzburgites and, less frequent, wehrlites and olivine-free pyroxenites (Hirschmann and Stolper 1996 and references therein). Such heterogeneities melt at different temperatures and cause different primary melt compositions during partial mantle melting. Before such heterogeneous melts may gain the surface they potentially evolve and mix with the volumetrically dominant melts from lherzolites. The original signature of melts from non-lherzolitic sources is thus often diluted by melts of dominantly peridotitic mantle and might even remain undetectable, not only in their major element composition but also when examining trace element signatures (e.g., Pertermann and Hirschmann 2003). Therefore, the role of mantle heterogeneities in the chemistry of erupted basalts remains a matter of debate.

Ultracalcic primitive magmas are characterized by high CaO-contents (13.5 to ~19.0 wt%) and high CaO/Al_2O_3 ratios (1.0 to ~1.8). They cannot be formed from fertile peridotites (Della-Pasqua and Varne 1997; Schiano et al. 2000; Kogiso and Hirschmann 2001; Schmidt et al. 2004) as they strongly contrast with experimental melts of lherzolitic lithologies under anhydrous or hydrous conditions (e.g., Falloon and Green 1988; Baker and Stolper 1994; Hirose and Kawamoto 1995; Fig. 1). Ultracalcic melts have been documented as whole-rock samples and melt inclusions in many geodynamic settings including mid-ocean-ridges, back-arc basins, oceanic islands and volcanic arcs (see Schiano et al. 2000 and references therein; Sigurdsson et al. 2000). Ultracalcic liquids preserved as quench glass inclusions are commonly MgO-rich and are often hosted

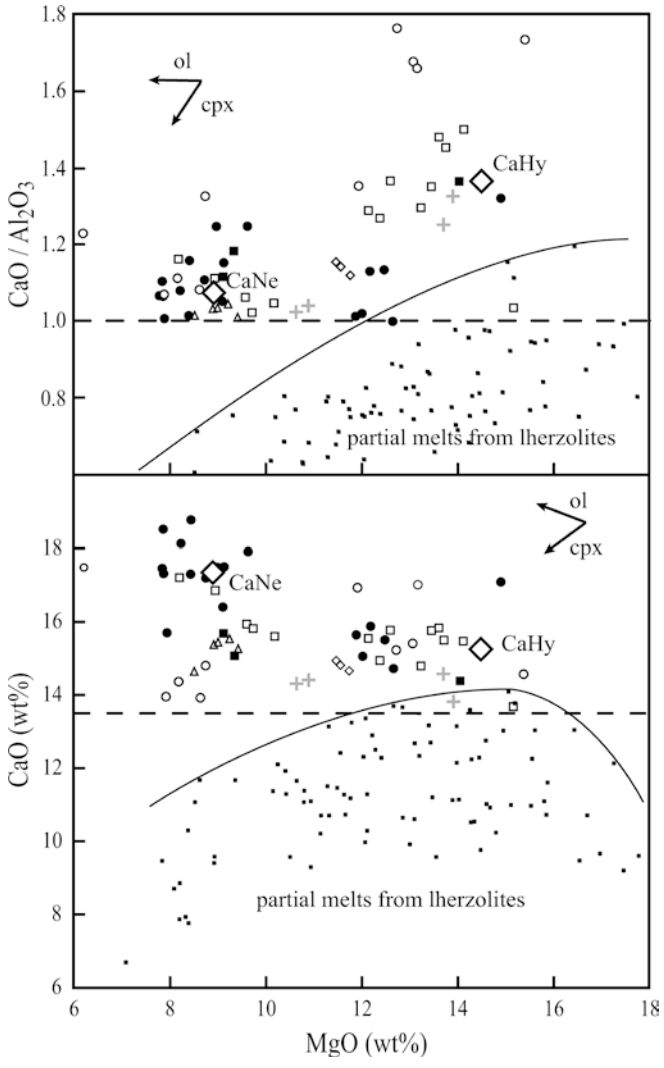

Fig. 1 CaO vs. MgO and CaO/Al_2O_3 vs. MgO plots for ultracalcic melt inclusions and whole-rocks. Nepheline-normative: *filled circle* arc melt inclusions (Schiano et al. 2000; de Hoog et al. 2001; Della-Pasqua and Varne 1997); *filled square* arc lavas (compilation in Schiano et al. 2000). Hypersthene normative: *open circle* inclusions from Lau Basin (Kamenetsky et al. 1997); *open square* inclusions from Iceland (Sigurdsson et al. 2000; Slater et al. 2001); *open diamond* inclusions from 43°N MAR (Kamenetsky et al. 1998); *open triangle* glass from Iceland (Trønnes 1990); + lavas from the Vanuatu arc (Barsdell and Berry 1990). *Arrows* show the effect of clinopyroxene and olivine fractionation. Experimental partial melts of lherzolite at 0.5–2.0 GPa are also shown for comparison (e.g., Falloon and Green 1988; Hirose and Kushiro 1993; Baker and Stolper 1994 corrected by Hirschmann et al. 1998; Kushiro 1996; Schwab and Johnston 2001; Wasylenki et al. 2003; Laporte et al. 2004). CaHy and CaNe are the two investigated compositions

in primitive phenocrysts (for example olivine $Fo_{87.6}$–$Fo_{92.1}$, Kamenetsky et al. 1997; Schiano et al. 2000). Ultracalcic lavas commonly contain phenocrysts with compositions characteristic for primitive mantle (e.g., olivine up to $Fo_{92.2}$, Barsdell and Berry 1990) suggesting either a primitive character or a simple and limited fractionation history of these magmas. Thus, the genesis of ultracalcic melts has been attributed to: (1) melting of carbonated or (CO_2 + H_2O)-fluxed lherzolites (Della-Pasqua and Varne 1997; Green et al. 2004), (2) interactions between picritic melts and clinopyroxene-rich lithologies (Trønnes 1990; Kamenetsky et al. 1998), (3) melting of pyroxenitic or wehrlitic lithologies (Barsdell and Berry 1990; Schiano et al. 2000; Kogiso and Hirschmann 2001) or (4) melting of depleted lherzolites (Kogiso and Hirschmann 2001; Schmidt et al. 2004).

In this study, the term "ultracalcic melts" is employed for melts with Mg-numbers (Mg# = 100×Mg/(Mg + Fe)) greater than 60, more than 13.5 wt% CaO, and CaO/Al_2O_3 ratios higher than 1.0. Mainly based on their silica vs. alkali contents, two distinct populations of ultracalcic magmas may be defined (Fig. 2, see also Kogiso and Hirschmann 2001): a silica-poor (typically 44–47 wt%) and alkali-rich (≥3.0 wt%) *nepheline-normative* population exclusively found in arc settings (Schiano et al. 2000); and a silica-rich (typically 48–53 wt%), alkali-poor (≤ 2.2 wt%) *hypersthene-normative* population found at mid-ocean ridges (Kamenetsky et al. 1998), ocean islands (Sigurdsson et al. 2000), and back-arc basins (Kamenetsky et al. 1997). Hypersthene-normative ultracalcic lavas have also been found in island-arc settings (Barsdell and Berry 1990). It should be noted that any of the definitions of "ultracalcic" exclusively based on major elements also classifies melilitites and nephelinites mainly occurring in intraplate settings (e.g., Dunworth and Wilson 1998) as ultracalcic melts. A number of studies have shown that such magmas may be derived as small melt fractions from garnet

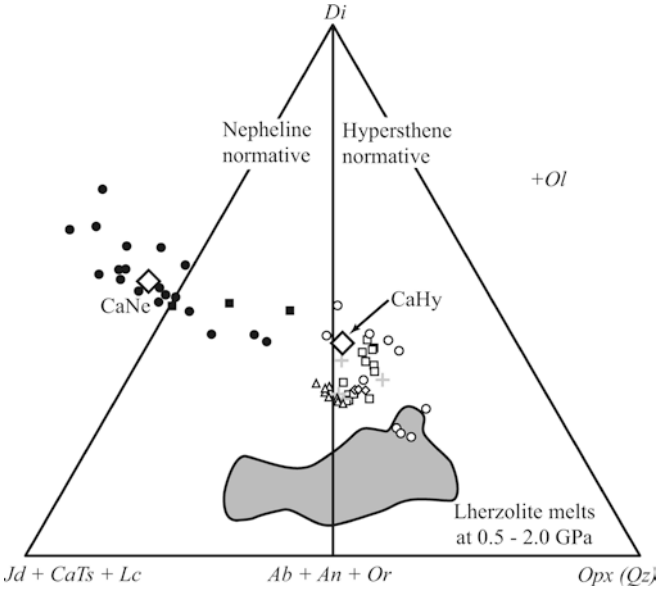

Fig. 2 Ternary diagram comparing data for ultracalcic inclusions and whole-rocks with liquids produced by experiments on lherzolites. Molecular normative projection from Ol onto the Di-Qz-Jd + CaTs + Lc face of the "basalt tetrahedron", after Falloon and Green (1988). Same symbols as Fig. 1. Field of experimental lherzolite melts at 0.5–2.0 GPa from Falloon and Green (1988), Hirose and Kushiro (1993), Baker and Stolper (1994) corrected by Hirschmann et al. (1998), Kushiro (1996), Schwab and Johnston (2001), Wasylenki et al. (2003), and Laporte et al. (2004)

lherzolite at 2.5–3.5 GPa with CO_2 + H_2O dissolved in the melt (e.g., Brey and Green 1977). The expansion of the garnet and orthopyroxene saturation volume due to the solubility of CO_2 at such high-pressure conditions is responsible for generation of CaO-rich, Al_2O_3- and SiO_2-poor melts. However, these conditions and residual phases result in a highly enriched trace element signature clearly distinct from the ultracalcic melts investigated and intended here (Kamenetsky et al. 1998; Schiano et al. 2000). In the following, the term ''ultracalcic melts'' will thus only refer to the two types defined above, excluding melilitites and nephelinites, whose study is beyond the scope of this paper.

Most ultracalcic melts are preserved as glasses in the form of melt inclusions inside phenocrysts in basalts. Although it is not the purpose of this study to discuss the principal significance of melt inclusions, it should be pointed out, that, when carefully homogenized and corrected for host olivine contamination, melt inclusions in olivines provide a window into magma generation processes such as partial melting, magma differentiation and mixing, and melt/wall-rock interactions. In the particular case of ultracalcic melt inclusions hosted in olivine which in turn is contained in melts with less extreme CaO-contents, any post-entrapment reaction with the host phase and diffusive re-equilibration process should lower CaO-contents (e.g., Gaetani et al. 2002), such that the present day composition would represent a less extreme melt chemistry. In the absence of post-entrapment reequilibration processes, it still remains uncertain whether ultracalcic melts reflect microscale processes documented in melt inclusions, or macroscale processes recorded in lavas and melt inclusions, or both. Both types of processes could be investigated by means of high-pressure equilibrium studies. Furthermore, ultracalcic magmas erupted as whole-rocks in various plate boundary settings (e.g., Schiano et al. 2000) have similar compositional arrays as melt inclusions (Figs. 1 and 2)

The aim of this study is to determine liquidus temperatures for ultracalcic liquids under volatile-absent conditions, secondly, whether such liquids have been in equilibrium with mantle lithologies, and third, pressure conditions of their eventual equilibration with their source. For this purpose, high-pressure, high-temperature experiments were performed on two model ultracalcic compositions, i.e. a hypersthene-normative and a nepheline-normative composition, following the inverse experimental approach (BVSP 1981). In such an approach, the phase relationships of a near-primary liquid are investigated as functions of temperature and pressure.

Experimental techniques

Starting materials

Fluid-absent liquidus experiments were performed on two extreme compositions of the ultracalcic array: a primitive hypersthene-normative ultracalcic liquid (composition CaHy; Sigurdsson et al. 2000; Barsdell and Berry 1990; Figs. 1 and 2, Table 1) and a primitive nepheline-normative ultracalcic liquid (composition CaNe; Schiano et al. 2000). The CaHy starting material was mixed from analytical grade oxides, synthetic feldspars, diopside, and fayalite. CaNe is a glass made from oxides and carbonates fused in a 1-atmosphere quench-furnace at controlled oxygen fugacity conditions. The fO_2 was adjusted such that the resulting Fe^{3+}/Fe^{total}-ratio was 0.2. Phase relations of the nepheline-normative ultracalcic liquid were further investigated on two compositions with 2.5 or 5 wt% olivine added (CaNe + 2.5 and CaNe + 5). For this purpose, natural gem quality olivine from Burma ($Fo_{90.9}$) and synthetic fayalite were mixed such that the added bulk olivine had a $Fo_{88.9}$ composition. All starting materials were ground under ethanol to fine powders (< 15 μm) and dried for at least 6 h at 140°C before loading.

Experimental methods

Depending on pressure, anhydrous experiments were performed either in a 1-atm CO_2/H_2 gas-mixing quench

Table 1 Composition of starting materials (wt%)

	Hypersthene-normative			Nepheline-normative			
	CaHy[a]	Epi[b]	Iceland[b]	CaNe[a]	CaNe + 2.5[a]	CaNe + 5[a]	Batan[b]
SiO_2	49.65 (39)	49.17	50.25	45.63 (61)	45.61 (36)	45.42 (54)	45.29
TiO_2	0.40 (15)	0.38	0.40	0.70 (08)	0.65 (12)	0.65 (10)	0.68
Al_2O_3	11.18 (23)	11.02	10.20	16.42 (38)	16.10 (37)	15.59 (31)	16.72
Cr_2O_3			1.40	0.09 (07)	0.09 (09)	0.07 (08)	
FeO	7.59 (16)	8.74	7.27	7.34 (40)	7.32 (33)	7.51 (29)	7.18
MgO	14.53 (42)	14.56	13.95	8.79 (30)	9.64 (28)	10.48 (26)	8.42
CaO	15.25 (42)	14.81	15.31	17.48 (55)	17.27 (34)	17.03 (32)	18.11
Na_2O	1.12 (17)	1.02	1.19	2.61 (14)	2.48 (17)	2.43 (15)	2.61
K_2O	0.28 (07)	0.29	0.02	0.94 (08)	0.84 (09)	0.82 (16)	0.99

[a]Mean analysis of melts in superliquidus experiments; the numbers in parenthesis are 2σ standard deviations, given in term of the last unit cited

[b]Representative ultracalcic melts: *Epi* Western Epi parental magma (Barsdell and Berry 1990); *Iceland* melt inclusion in spinel from Borgarhraun (Sigurdsson et al. 2000); *Batan* mean composition of melt inclusions in B7 olivine (Schiano et al. 2000)

furnace; to 0.7 GPa in an internally heated pressure vessel; and from 0.7 to 1.5 GPa in single-stage piston-cylinder apparatus with 19.1 or 12.7 mm bores. 1-atmosphere experiments were performed using the Pt-wire loop technique. For high-pressure experiments, double capsules composed of an inner graphite container and an outer platinum capsule were employed. Piston-cylinder experiments were performed with NaCl-Pyrex-graphite-MgO assemblies. Temperature was measured using either a $W_{74}Re_{26}/W_{95}Re_5$ (piston cylinder) or a $Pt_{90}Rh_{10}/Pt_{70}Rh_{30}$ thermocouple (internally heated pressure vessel and 1-atm furnace) and was maintained within 1°C of the setpoint value. In some of the early experiments (experiments ak02–ak14, Table 2), temperatures were corrected for a slight temperature difference between charge and thermocouple, caused by

Table 2 Experimental run data

Experiments	P (GPa)	T (°C)	Time (h)	Glass	Olivine	Cpx	Plagio	Spinel	r^2
CaHy starting composition									
ak27	0.70	1,350	2.6	0.88 (3)	0.05 (2)	0.07 (3)			0.50
ak28	0.70	1,365	6.1	0.92 (3)	0.04 (1)	0.05 (3)			0.09
ak30	0.70	1,373	4.0	0.98 (1)	0.02 (1)				0.37
ak26	0.70	1,375	4.0	1					
ak02	1.00	1,383 (1,400)[a]	70.2	0.75 (2)	0.03 (1)	0.22 (2)			0.17
ak29	1.01	1,390	6.0	0.92 (3)	0.01 (1)	0.07 (3)			0.02
ak03	1.00	1,412 (1,440)[a]	24.5	0.98 (1)	0.02 (1)				0.06
ak24	1.00	1,410	3.9	1					
ak14	1.21	1,386 (1,420)[a]	3.5	0.85 (3)	0.00 (1)	0.15 (3)			0.01
ak12	1.20	1,421 (1,450)[a]	3.9	1					
ak08	1.50	1,398 (1,450)[a]	15.2	0.60 (3)	0.00 (1)	0.40 (2)			0.12
ak34	1.50	1,420	5.0	0.84 (3)		0.16 (3)			0.63
ak31	1.50	1,450	6.0	1					
CaNe starting composition									
bt13	0.0001	1,180	6.0	0.72 (5)	0.03 (1)	0.14 (3)	0.12 (3)		0.07
bt12	0.0001	1,190	2.3	0.96 (5)	0.02 (1)	0.02 (1)	0.00 (3)		0.12
bt11	0.0001	1,200	4.0	0.99 (1) (6)	0.01 (1)			0.00 (1)	0.48
bt10	0.0001	1,210	4.1	1.00 (1)				0.00 (1)	
bt09	0.0001	1,220	4.0	1					
bt30	0.250	1,200	2.0	0.75 (5)	0.01 (2)	0.19 (3)	0.06 (4)		0.99[b]
bt42	0.250	1,220	4.0	1.00 (1)		0.00 (1)			0.12
bt29	0.250	1,220	2.0	1					
bt22	0.250	1,240	2.0	1					
bt08	0.500	1,175	60.0	x		x	x	x	
bt17	0.500	1,190	3.3	x		x			
bt05	0.500	1,220	111.5	x		x			
bt14	0.500	1,250	3.3	x		x			
bt18	0.500	1,257	4.0	0.97 (3)		0.03 (3)			0.09
bt21	0.500	1,270	4.0	1					
bt01	0.70	1,250	4.0	0.74 (3)		0.26 (3)		0.00 (1)	1.58[b]
bt03	0.70	1,275	4.1	0.90 (3)		0.10 (3)			0.57
bt35	0.700	1,285	3.0	x		x			
bt02	0.70	1,300	4.7	1					
CaNe + 2.5 starting composition									
bt39	0.0001	1,230	4.0	1.00 (1)	0.00 (1)			0.00 (1)	0.85
bt37	0.0001	1,240	4.0	1					
bt31	0.250	1,200	2.0	0.68 (1)	0.04 (1)	0.19 (3)	0.09 (3)		0.56
bt27	0.250	1,220	2.0	0.96 (1)	0.04 (1)				0.55
bt23	0.250	1,240	2.0	0.98 (1)	0.02 (1)				0.38
bt40	0.500	1,250	4.4	x	x	x			
bt19	0.500	1,270	4.0	1.00 (1)	0.00 (1)				0.32
bt36	0.70	1,285	4.0	0.84 (3)		0.16 (3)			1.78[b]
bt38	0.70	1,300	3.0	1					
CaNe + 5 starting composition									
bt45	0.0001	1,240	4.0	0.99 (1)	0.01 (1)				1.53[c]
bt44	0.0001	1,250	4.0	1					
bt24	0.250	1,240	2.0	0.95 (1)	0.05 (1)				0.18
bt15	0.500	1,250	3.0	x	x	x			
bt20	0.500	1,270	4.0	x	x	x			
bt33	0.700	1,285	4.0	x	x	x			

x glasses are not measurable, thus mass balance calculations cannot be performed

[a]These temperatures are corrected for a temperature difference between thermocouple and sample. The numbers in parentheses are the initial uncorrected temperatures

[b]$r^2 \geq 1$ indicate that melts have been quench-modified, in experiments with a large amount of crystals

[c]This experiment suffered ~10% iron loss

a larger-than-normal distance between the two. This correction has been calibrated by determining the axial thermal profile of the assembly through two-thermocouple experiments. Overall, the thermal gradient in the capsule is less than 15°C in piston cylinder experiments, and almost negligible in the internally heated pressure-vessel and the one-atmosphere furnace experiments. The temperature accuracy is thought to be at least within ±15°C. For piston-cylinder experiments, a pressure correction was found to be not necessary and an uncertainty of 0.05 GPa is assumed on the nominal pressure (Vielzeuf and Clemens 1992). For internally heated pressure-vessel experiments, pressure uncertainties do not exceed 5 MPa. Most run durations were 2–24 h, initially longer run times have subsequently been shortened to the minimum time necessary for equilibration.

Oxygen fugacity

The presence of graphite in high-pressure experiments delimits oxygen fugacities to maximum values of the graphite-CO buffer without placing a lower limit on fO_2 (Holloway et al. 1992). The first experiments at low pressure (0.25 GPa), long run durations (4 days) and with relatively reduced starting material ($Fe^{3+}/Fe^{total} = 0.1$), have resulted in iron droplets within the silicate liquid. This implies an oxygen fugacity at the iron-wüstite buffer, and in order to maintain oxygen fugacities realistic for mantle melting processes, we used shorter run times and slightly oxidized starting materials: all subsequent starting materials had Fe^{3+}/Fe^{total} ratios of 0.2.

Experimental fO_2 and CO_2 contents of the glass were estimated employing the model of Holloway et al. (1992). At the experimental conditions, CaHy glasses should have a Fe^{3+}/Fe^{tot} of 0.04–0.05, a CO_2 content of 0.18 wt%, and a fO_2 near QFM-2.5 (QFM from O'Neill 1987). However, calculated Fe/Mg olivine-liquid distribution coefficients are in accordance to the predicted value of 0.32 at 1.0 GPa (Ulmer 1989) when assuming all Fe as divalent (Table 3). This suggests that at 1400°C, almost all of the initial Fe^{3+} is reduced to Fe^{2+} within 4 h run duration. As metallic iron was not observed, oxygen fugacities are still above the IW oxygen buffer (near QFM-3.7, O'Neill and Pownceby 1993).

Experiments with the CaNe, CaNe + 2.5 and CaNe + 5 starting materials were performed at lower temperatures and pressures than with the hypersthene-normative starting material. For these experimental melts, the model of Holloway et al. (1992) in combination with CO_2 solubility data for Ca-rich nepheline-normative liquids (Thibault and Holloway 1994), results in Fe^{3+}/Fe^{tot} ratios of ~0.05, CO_2 contents of 0.17 wt%, and an fO_2 near QFM-2.9. Fe/Mg olivine-liquid distribution coefficients calculated with the estimated Fe^{3+}/Fe^{tot} coincide to the predicted values of 0.30–0.31 within uncertainty (Ulmer 1989; Table 4). In order to assure the internal consistency of the experimental set, oxygen fugacities in the 1-atm experiments were held at QFM-2.0.

The dissolved CO_2 in the experimental melts cannot be avoided in experiments making use of graphite capsules. However, the relatively low calculated CO_2 concentrations will have little influence on phase relations. It should be noted that, according to Jambon (1994) and Gerlach and Graeber (1985), primitive MORB and Kilauean magmas have 0.13 and 0.65 wt% CO_2, respectively.

Analytical conditions

Compositions of crystalline phases and glasses were determined with a Cameca SX100 electron microprobe at the Laboratoire Magmas et Volcans. For crystalline phases, a 15 kV accelerating voltage and a 15 nA beam current were employed, counting times were 10 s and the electron beam was focussed. For glass analyses, the beam current was lowered to 8 nA and the beam was spread to 10 μm diameter. Uncertainties given in parentheses after the mean value in Tables 3 and 4 are 2σ absolute errors for electron microprobe analyses (Ancey et al. 1978), given in terms of the last unit cited. For all experiments, phase proportions were calculated by mass balance, following Albarède and Provost (1977).

Attainment of equilibrium

Equilibration in the oxide-mix starting material (Table 2) was tested with a few long experiments that yielded phase compositions coherent with their next nearest neighbours in P-T space. In the oxide-mix, two phases were present both in the starting material (pure diopside and fayalite) and run products (clinopyroxene and olivine), nevertheless, olivines resulted unzoned and only one experiment (ak14) contained a few single clinopyroxenes with 5 μm diameter Ca- and Mg-rich cores easily distinguished from equilibrium rims. In the glassy starting material, all phases crystallized anew, and direct approach to run temperature and overstepping of the liquidus with subsequent equilibration at run temperature yielded identical results. Rare residual olivine cores were observed in olivine addition experiments (CaNe + 2.5 and CaNe + 5 starting materials). With the exception of the few residual clinopyroxene and olivine cores, there is no evidence for diffusional reequilibration and generally the starting materials had to react completely (e.g., fayalite dissolved in the melt which precipitated olivines with X_{Mg} ranging from 0.87 to 0.91 in the different experiments).

Crystals show idiomorphic equilibrium textures (Fig. 3), with the exception of some easily identifiable quench growth rims and dendritic quench crystals. Crystallisation of large amounts of aluminous quench

Table 3 Average compositions of solid phases and glasses in liquidus experiments on ultracalcic hypersthene-normative composition CaHy

	P (GPa)	T (°C)	Experiments	SiO_2	TiO_2	Al_2O_3	FeO*	MgO	CaO	Na_2O	K_2O	Total	Mg#	Ca pfu	Kd[a]
Olivine	0.70	1,365	ak28	40.97 (46)		0.04 (05)	9.22 (26)	49.12 (57)	0.61 (08)			100.80	90.5 (3)	0.016 (2)	0.314 (34)
	0.70	1,375	ak30	40.97 (46)		0.05 (05)	8.89 (22)	49.51 (57)	0.53 (08)			99.10	90.8 (3)	0.014 (2)	0.318 (37)
	1.00	1,383	ak02	40.45 (45)		0.06 (05)	10.83 (26	48.14 (56)	0.47 (08)			100.70	88.8 (4)	0.013 (2)	0.307 (32)
	1.00	1,390	ak29	41.50 (51)		0.05 (05)	9.05 (32)	49.71 (57)	0.53 (08)			100.85	90.7 (4)	0.014 (2)	0.321 (33)
	1.00	1,412	ak03	41.35 (47)		0.07 (05)	8.79 (27)	49.21 (57)	0.54 (08)			99.08	90.9 (4)	0.014 (2)	0.327 (36)
	1.20	1,386	ak14	40.98 (66)		0.09 (05)	9.99 (24)	48.40 (60)	0.51 (08)			99.06	89.6 (3)	0.014 (2)	0.337 (35)
	1.50	1,398	ak08	39.80 (44)		0.16 (12)	12.91 (17)	46.60 (20)	0.48 (08)			98.63	86.6 (4)	0.013 (2)	0.346 (36)
Cpx	0.70	1,365	ak28	54.72 (56)	0.09 (10)	1.92 (50)	2.90 (21)	19.94 (42)	20.28 (42)	0.15 (06)		100.36	92.5 (7)	0.782 (16)	
	1.00	1,383	ak02	53.13 (54)	0.14 (10)	3.61 (65)	3.46 (21)	18.68 (50)	20.78 (47)	0.19 (06)		100.12	90.6 (7)	0.803 (16)	
	1.00	1,390	ak29	54.08 (60)	0.13 (10)	3.27 (19)	2.90 (14)	19.90 (50)	19.54 (63)	0.19 (06)		100.08	92.5 (5)	0.752 (24)	
	1.20	1,386	ak14	53.37 (54)	0.14 (10)	3.81 (35)	3.30 (16)	19.20 (62)	19.95 (41)	0.22 (06)		99.97	91.2 (6)	0.769 (16)	
	1.50	1,398	ak08	51.75 (69)	0.21 (10)	6.52 (65)	4.14 (21)	18.13 (50)	18.88 (47)	0.36 (06)		100.34	88.6 (10)	0.729 (18)	
	1.50	1,420	ak34	53.43 (54)	0.14 (10)	4.05 (57)	3.52 (17)	19.04 (59)	19.54 (65)	0.27 (06)		99.73	90.6 (7)	0.754 (25)	
Glass	0.70	1,365	ak28	49.46 (63)	0.41 (09)	12.12 (25)	7.76 (31)	12.98 (35)	15.72 (44)	1.26 (09)	0.29 (9)	100.43	74.9 (13)		
	0.70	1,373	ak30	49.38 (63)	0.45 (09)	11.59 (24)	7.88 (32)	13.96 (38)	15.31 (46)	1.13 (08)	0.29 (6)	99.13	76.0 (12)		
	1.00	1,383	ak02	48.64 (62)	0.51 (12)	13.85 (40)	8.72 (35)	11.91 (32)	14.63 (41)	1.39 (16)	0.35 (6)	98.72	70.9 (14)		
	1.00	1,390	ak29	49.33 (63)	0.40 (11)	11.97 (24)	7.83 (32)	13.83 (38)	15.11 (42)	1.20 (09)	0.31 (9)	98.60	75.9 (12)		
	1.00	1,412	ak03	49.76 (64)	0.41 (18)	11.51 (23)	7.59 (31)	13.89 (38)	15.35 (43)	1.21 (08)	0.28 (6)	100.08	76.5 (12)		
	1.20	1,386	ak14	49.01 (63)	0.43 (08)	12.49 (25)	8.38 (36)	13.68 (43)	14.38 (40)	1.33 (16)	0.29 (9)	99.36	74.4 (14)		
	1.50	1,398	ak08	47.86 (61)	0.53 (10)	14.26 (29)	10.03 (40)	12.52 (34)	12.76 (36)	1.59 (11)	0.44 (6)	100.07	69.0 (14)		
	1.50	1,420	ak34	49.56 (63)	0.48 (09)	12.81 (26)	7.95 (32)	13.17 (36)	14.46 (40)	1.24 (08)	0.32 (6)	99.00	74.7 (13)		

The numbers in parentheses are 2σ standard deviations, given in term of the last unit cited

[a]Calculated assuming all Fe is divalent

Table 4 Representative average compositions of solid phases and glasses in liquidus experiments on ultracalcic nepheline-normative compositions CaNe, CaNe + 2.5, CaNe + 5

		P (GPa)	T (°C)	Experiments	SiO_2	TiO_2	Al_2O_3	Cr_2O_3	FeO*	MgO	CaO	Na_2O	K_2O	Total	Mg#	Ca pfu	Kd[a]
Olivine	CaNe	0.0001	1,190	bt12	40.62 (45)		0.11 (5)	0.08 (9)	11.13 (36)	46.96 (54)	1.04 (11)			98.73	88.3 (5)	0.028 (3)	0.27 (3)
		0.0001	1,200	bt11	40.73 (45)		0.08 (5)	0.06 (9)	10.29 (25)	47.80 (55)	1.02 (11)			99.59	89.2 (3)	0.027 (3)	0.30 (3)
		0.250	1,200	bt30	39.67 (44)		0.10 (5)	0.02 (9)	12.66 (31)	46.59 (54)	0.90 (10)			100.56	86.8 (4)	0.024 (3)	0.24 (3)[d]
	CaNe + 2.5	0.0001	1,230	bt39	40.18 (45)		0.11 (5)	0.12 (9)	9.56 (23)	49.19 (57)	0.82 (10)			101.13	90.2 (3)	0.021 (3)	0.30 (3)
		0.250	1,200	bt31	40.77 (23)		NA	NA	11.96 (41)	47.28 (74)	NA			99.40	87.6 (9)		0.21 (3)
		0.250	1,240	bt23	40.55 (46)		0.06 (5)	0.07 (9)	10.41 (25)	48.13 (56)	0.74 (12)			101.34	89.2 (3)	0.019 (3)	0.29 (3)
		0.50	1,270	bt19	40.09 (45)		0.04 (5)	0.06 (9)	9.83 (24)	49.27 (58)	0.66 (8)			101.22	89.9 (3)	0.017 (2)	0.28 (3)
	CaNe + 5	0.0001	1,240	bt45	40.94 (45)		0.06 (5)	0.08 (9)	9.37 (23)	48.78 (56)	0.74 (8)			99.48	90.3 (3)	0.019 (2)	0.31 (3)
		0.70	1,285	bt33	41.05 (46)		0.06 (6)	0.04 (9)	10.41 (44)	47.85 (66)	0.52 (22)			99.14	89.1 (5)	0.014 (3)	
Cpx	CaNe	0.0001	1,190	bt12	51.19 (52)	0.41 (10)	4.64 (25)	0.95 (17)	2.76 (16)	15.77 (29)	24.06 (49)	0.19 (6)		99.65	91.0 (5)	0.940 (19)	
		0.250	1,200	bt30	51.45 (54)	0.44 (10)	4.94 (48)	0.35 (34)	2.92 (19)	16.01 (28)	23.68 (48)	0.20 (6)		100.04	90.7 (7)	0.923 (19)	
		0.250	1,220	bt42	51.56 (52)	0.41 (10)	4.96 (22)	0.75 (14)	2.68 (13)	16.21 (34)	23.26 (47)	0.16 (6)		99.93	91.5 (5)	0.907 (18)	
		0.500	1,250	bt14	49.68 (51)	0.51 (10)	7.94 (53)	0.58 (32)	3.10 (48)	14.53 (38)	23.23 (82)	0.41 (32)		99.77	89.3 (9)	0.906 (32)	
		0.500	1,257	bt18	50.96 (57)	0.42 (11)	6.05 (41)	0.50 (10)	2.97 (38)	15.69 (33)	23.09 (72)	0.28 (7)		100.31	90.4 (9)	0.900 (18)	
		0.70	1,250	bt01	49.72 (51)	0.49 (11)	8.87 (18)	0.31 (8)	2.86 (14)	14.27 (25)	22.59 (46)	0.65 (8)		100.71	89.9 (6)	0.879 (18)	
		0.70	1,275	bt03	51.55 (52)	0.44 (10)	6.09 (32)	0.35 (8)	2.51 (12)	15.27 (26)	23.46 (47)	0.30 (6)		98.73	91.5 (5)	0.914 (18)	
		0.70	1,285	bt35	50.12 (54)	0.40 (10)	6.89 (53)	0.41 (13)	2.98 (20)	15.10 (39)	23.70 (48)	0.36 (8)		100.74	90.0 (8)	0.923 (19)	
	CaNe + 2.5	0.250	1,200	bt31	51.34 (52)	0.40 (10)	4.97 (10)	0.59 (11)	3.03 (14)	15.83 (27)	23.64 (48)	0.18 (6)		99.84	90.3 (6)	0.923 (19)	
		0.500	1,250	bt40	51.42 (56)	0.44 (10)	6.18 (47)	0.11 (8)	2.83 (23)	15.33 (37)	23.12 (47)	0.23 (6)		100.12	89.7 (6)	0.902 (18)	
		0.70	1,285	bt36	50.88 (52)	0.32 (10)	5.41 (32)	0.48 (9)	2.86 (13)	16.70 (29)	23.06 (48)	0.27 (6)		99.54	91.2 (5)	0.895 (18)	
	CaNe + 5	0.70	1,285	bt33	51.18 (52)	0.35 (10)	5.77 (15)	0.47 (9)	2.81 (15)	15.62 (27)	23.44 (48)	0.34 (6)		99.94	90.8 (5)	0.913 (19)	
Pl	CaNe	0.0001	1,190	bt12	46.13 (48)		33.72 (36)		0.47 (8)	0.23 (10)	18.04 (40)	1.32 (16)	0.11 (8)	99.05		0.889 (21)	
		0.250	1,200	bt30[b]	48.53 (52)		32.35 (34)		0.17 (8)	–	16.98 (34)	1.82 (17)	0.03 (5)	97.45		0.837 (18)	
	CaNe + 2.5	0.250	1,200	bt31[b]	48.53 (51)		32.47 (33)		0.00 (8)	–	16.96 (38)	1.92 (13)	0.11 (5)	98.64		0.835 (20)	
Glass	CaNe	0.0001	1,190	bt12	45.78 (59)	0.70 (13)	16.85 (34)		7.60 (31)	8.02 (22)	17.66 (50)	2.51 (17)	0.85 (10)	98.38	65.3 (15)		
		0.0001	1,200	bt11	46.04 (59)	0.72 (13)	16.65 (34)		6.78 (29)	8.65 (24)	17.99 (51)	2.34 (19)	0.78 (9)	98.77	69.5 (15)		
		0.250	1,200	bt30	44.97 (58)	0.68 (12)	18.00 (37)		8.58 (35)	7.21 (37)	15.57 (51)	3.89 (26)	1.11 (13)	99.25	60.0 (22)[d]		
		0.250	1,220	bt42	45.41 (58)	0.66 (12)	16.51 (34)		7.15 (29)	8.93 (24)	17.48 (49)	2.64 (18)	0.90 (11)	98.41	69.0 (15)		
		0.500	1,257	bt18	45.55 (58)	0.68 (13)	16.52 (34)		7.57 (31)	8.46 (23)	17.47 (49)	2.72 (22)	0.98 (12)	98.07	66.6 (15)		
		0.70	1,250	bt01	45.30 (58)	0.65 (12)	18.63 (38)		8.02 (32)	7.19 (20)	15.03 (43)	3.79 (26)	1.36 (16)	100.41	61.5 (16)[d]		
		0.70	1,275	bt03	45.64 (58)	0.69 (13)	17.40 (36)		7.20 (29)	7.96 (22)	16.98 (48)	3.01 (20)	1.04 (12)	99.27	66.3 (15)		
	CaNe + 2.55	0.0001	1,210	bt39	45.95 (59)	0.71 (13)	16.05 (33)		7.01 (28)	9.92 (27)	17.68 (50)	1.89 (13)	0.66 (09)	99.77	71.6 (14)		
		0.250	1,200	bt31	44.52 (55)	0.77 (14)	17.74 (35)		8.78 (34)	6.83 (18)	16.17 (44)	4.00 (26)	1.18 (14)	96.38	58.1 (16)[d]		
		0.250	1,240	bt23	45.71 (58)	0.70 (13)	16.11 (33)		7.31 (29)	9.38 (26)	17.16 (48)	2.69 (18)	0.86 (10)	100.45	69.6 (14)		
		0.500	1,270	bt19	45.69 (58)	0.63 (12)	15.80 (32)		7.53 (30)	9.88 (27)	16.95 (47)	2.56 (17)	0.89 (11)	99.43	70.1 (14)		
		0.70	1,285	bt36	44.29 (57)	0.69 (13)	17.43 (36)		9.04 (36)	8.82 (24)	15.31 (43)	3.29 (22)	1.11 (13)	97.42	63.5 (16)[d]		
	CaNe + 5	0.0001	1,240	bt45	46.25 (59)	0.67 (12)	16.22 (33)		6.81 (27)	10.06 (27)	17.34 (49)	1.89 (13)	0.67 (08)	99.83	72.5 (14)[c]		
Sp	CaNe	0.0001	1,200	bt11[b]	–	0.44	42.57	25.02	13.09	18.70	0.17	–	–	27.5	76.0		
		0.70	1,250	bt01[b]	–	0.16	62.69	2.28	10.11	23.13	1.62	–	–	2.4	80.3		

NA not analysed

[a]The numbers in parentheses are 2σ standard deviations, given in term of the last unit cited

[b]Analysed spinel and plagioclase crystals are tiny (max. 2–3 μm) and their microprobe analyses overlap the surrounding liquid, so analyses have been corrected by substracting an adequate amount of liquid composition

[c]This experiment suffered minor (< 10%) iron loss

[d]Experiments were $r^2 \geq 1$, melts have been quench-modified so melt compositions are only indicative and olivine/melt Kd are not equilibrium values

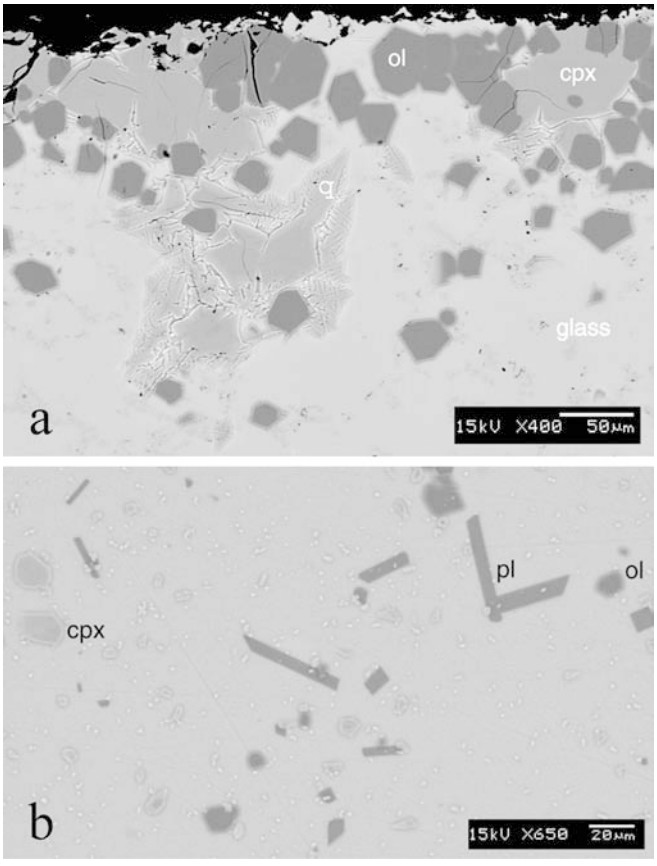

Fig. 3a, b SEM backscattered electron images of experimental products, **a** CaHy 1,365°C, 0.7 GPa, **b** CaNe, 1,190°C, 1 atm, showing equilibrium clinopyroxene (*cpx*), olivine (*ol*) and plagioclase (*pl*) phenocrysts. Quench clinopyroxene (*q*) appears in most of the experiments. The clear zoning in the right image is due to a slight thermal gradient (~5°C)

clinopyroxenes (enriched in Ca-Tschermaks component) occurs in some internally heated pressure vessel experiments as a consequence of the low quench rate in this apparatus. In these experiments, clinopyroxene analyses were carefully sorted to exclude quench-related compositions. To control chemical equilibration, olivine-liquid Fe–Mg distribution coefficients were calculated when possible. With the exception of bt30 and bt31, they agree within error to the predicted values (Ulmer 1989). In the experiment bt30, only one olivine crystal is observable and the liquid is probably affected by some quench modification related to the high proportion of solids. The corresponding olivine composition and calculated Kd value (0.24) are reported in Table 4, but the calculated phase proportions in this experiment are deemed as unreliable.

Liquidus conditions and mineralogy

For all of the investigated bulk compositions, olivine is the low pressure and clinopyroxene the high pressure liquidus phase (Figs. 4 and 5). Multiple saturation in

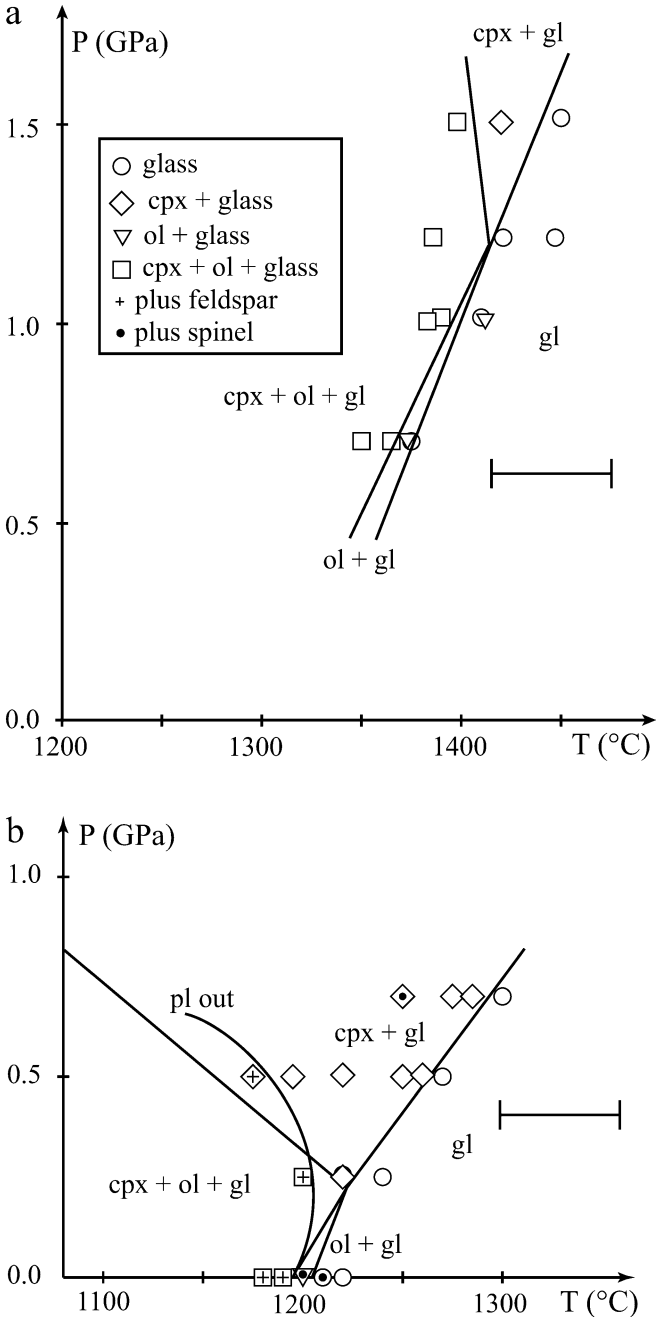

Fig. 4a, b Experimentally determined liquidus surfaces for two model ultracalcic primitive liquids: **a** CaHy is silica-rich and hypersthene normative; **b** CaNe is silica-poor and nepheline-normative. CaHy is multiply saturated in olivine and clinopyroxene at 1.2 GPa–1,410°C; CaNe is multiply saturated in olivine and clinopyroxene at pressures near 0.2 GPa and 1,220°C

olivine + orthopyroxene ± clinopyroxene, which is expected for equilibrium with a residual peridotite mineralogy, does not occur at or near the liquidus.

Hypersthene-normative ultracalcic composition

For the hypersthene normative composition CaHy, olivine is the low-pressure liquidus phase and is replaced

by clinopyroxene at higher pressures. Multiple saturation in olivine + clinopyroxene occurs on the liquidus at 1.2 GPa and 1,410°C (Fig. 4a). Orthopyroxene is never observed in our experiments.

The Mg of liquidus olivines vary between 90.9 and 89.6 near the multiple saturation point (Table 3). These values are compatible with a peridotitic mantle source (BVSP 1981; Baker and Stolper 1994). However, equilibrium olivines are richer in Ca (~0.5 wt% CaO) than typical mantle olivines (BVSP 1981) or olivines from lherzolite partial melting experiments (e.g., Baker and Stolper 1994; Schwab and Johnston 2001). The high Ca contents in our experimental olivines probably reflect the ultracalcic nature of the liquid. As Ca partition coefficients between olivine and melt correlate positively with CaO contents of the melt (Libourel 1999), Ca content in olivine increases rapidly with increasing CaO content of the equilibrium liquid. Similar high CaO contents have also been measured in olivines from partial melting experiments on wehrlites (Pickering-Witter and Johnston 2000; Kogiso and Hirschmann 2001; Schwab and Johnston 2001).

Liquidus clinopyroxenes (Mg# 91.7–93.3, Table 3) are alkali-poor relative to typical mantle clinopyroxenes (BVSP 1981; Baker and Stolper 1994). Alumina contents (1.9–4.0 wt% Al_2O_3) are low (compare Baker and Stolper 1994; Wasylenki et al. 2003) and compatible with a refractory source. The liquidus clinopyroxenes contain 0.72–0.81 Ca per formula unit (pfu), whereas clinopyroxenes on the two pyroxene solvus have 0.60–0.65 Ca pfu between 1.0 and 2.0 GPa at 1,400°C (Brey and Huth 1984). CaHy pyroxenes are thus 'far' from orthopyroxene saturation, even at the higher pressures investigated. It has been shown that the addition of H_2O or CO_2 to a basic magma increases orthopyroxene stability (Pichavant et al. 2002; Brey and Green 1977), however, experiments on a bulk composition similar to CaHy at 1.5 and 2 GPa under H_2O- and CO_2-bearing conditions failed to stabilize orthopyroxene and shows only clinopyroxene as a liquidus phase (Schmidt et al. 2004).

Summarizing, the multiple-saturation experiments demonstrate that the melt composition CaHy is not in equilibrium with a lherzolitic mantle residue and thus either represents a derivative melt or a melt from a non-lherzolitic lithology.

Nepheline-normative ultracalcic composition

For the nepheline-normative composition CaNe, olivine is the liquidus phase only at pressures ≤ 0.2 GPa (Fig. 4b), and clinopyroxene at pressures above 0.2 GPa. Multiple saturation in olivine + clinopyroxene occurs at a much lower pressure (0.2 GPa) and temperature (1,220°C) than for the hypersthene-normative composition CaHy. Orthopyroxene is never present at our experimental conditions. Ca-rich (An_{88}–An_{80}) plagioclase is observed slightly below the liquidus

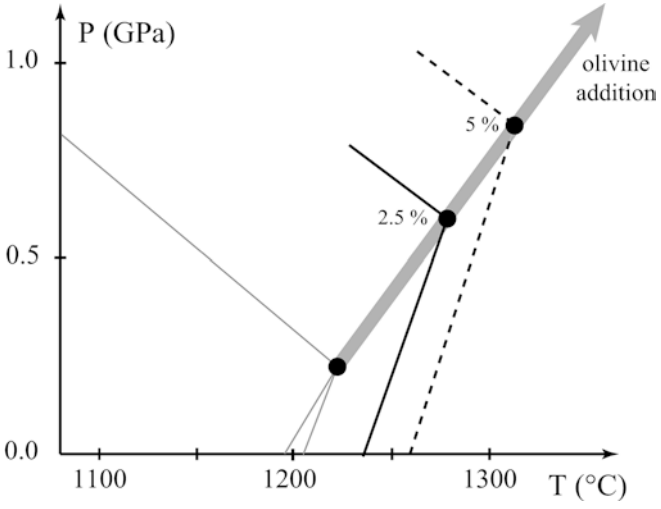

Fig. 5 Effect of olivine addition on the phase relations of a silica-poor nepheline-normative ultracalcic composition (CaNe). *Light lines* CaNe composition (compare to Fig. 4b); *full lines* CaNe + 2.5 wt% olivine added; *dotted lines*: CaNe + 5 wt% olivine added. With addition of olivine, the multiple saturation point migrates from 0.25 GPa-1,220°C to 0.6 GPa-1,275°C, and probably to ~0.8 GPa–1,310°C

at low pressures (0–0.2 GPa) but its stability field retracts away from the liquidus at higher pressure (Fig. 4b).

The experiments on the nepheline normative composition CaNe indicate that olivine-saturation is restricted to low pressures. The pressure range where olivine appears on the liquidus can be extended towards higher pressures by olivine addition which may be justified by incomplete correction for host mineral crystallisation or by supposing that the CaNe-liquid underwent some olivine fractionation. Addition of 2.5 wt% equilibrium olivine ($Fo_{88.9}$) is sufficient to increase the pressure of multiple saturation in olivine + clinopyroxene to 0.6 GPa at 1,275°C (Fig. 5); phase compositions are similar to those from experiments on the CaNe starting material, and orthopyroxene remains absent. Olivine addition of 5wt% was also tentatively tested, and the few experiments performed (Table 2, Fig. 5) suggest a further increase of the liquidus temperature at low pressures which then would result in a shift of the multiple saturation point to pressures higher than 0.6 GPa.

Liquidus olivines have lower Mg# (Mg# 89.2 for CaNe, Mg# 89.2–90.2 for CaNe + 2.5, Mg# 89.1–90.3 for CaNe + 5) than for CaHy, nevertheless, such values remain consistent with a mantle origin. Equilibrium olivines are more CaO-rich (up to 1.04 wt% CaO) than for CaHy composition. High CaO contents in olivine are related to the high CaO-content of the magma. However, we are not aware of such high CaO contents in olivine from melting experiments on lherzolitic lithologies. It should be noted that reported analyses of olivines hosting CaNe-like ultracalcic melt inclusions are generally not CaO-rich. However, there

is no evidence from published data that olivine crystals near the inclusions are not CaO-rich; in fact, De Hoog et al. (2001) reported an analysis of host olivine CaO contents as high as 0.93 wt%. At present, this problem remains unsolved, and a systematic study of olivine host compositions in the immediate vicinity of ultracalcic melt inclusions is required.

Clinopyroxenes near the multiple saturation point have lower Mg (Mg# 90.0–91.5, Table 4) and higher Al contents than in CaHy. These values would still be compatible with a mantle source, however, the experimentally produced Ca-rich clinopyroxenes (Table 4, 0.89–0.93 Ca pfu) are more than 0.2 Ca pfu from the two-pyroxene solvus (Brey and Huth 1984), suggesting that ultracalcic nepheline-normative melts are even further from orthopyroxene saturation than ultracalcic hypersthene-normative melts.

The role of spinel is difficult to assess in our experiments as spinel stability is strongly dependant on oxygen fugacities (Gust and Perfit 1987) and the oxygen fugacities imposed by the use of graphite capsules at such high temperatures are probably more reducing than during natural mantle melting processes. Cr-poor spinel is a liquidus phase in the one-atmosphere experiments, whereas almost Cr-free spinel occasionally occurs in some high-pressure experiments. Nevertheless it could not be excluded that higher oxygen fugacity will result in spinel being a liquidus or near-liquidus phase at high pressures.

Discussion: origin of ultracalcic melts

The contrasting P-T conditions of multiple saturation obtained for the hypersthene- and the nepheline-normative ultracalcic melts, together with their different chemical characteristics, suggest that they originate from different materials at quite distinct P-T conditions. The hypersthene normative CaHy melt appears to originate from a depleted source at mantle conditions and has a high liquidus temperature, whereas CaNe is a relatively alkali rich composition with lower CaO/Al_2O_3 ratio and liquidus temperature. From a compositional point of view, liquidus temperature differences (>100°C at 0.7 GPa) between the two compositions result from the fact that CaNe is poorer in MgO than CaHy (8.8 wt% vs. 14.5 wt%, Table 1), and from the alkali-rich nature of the CaNe melt, which is also likely to play a significant role (Soulard et al. 1992).

Our multiple saturation points have been derived from two extreme bulk compositions to obtain extreme conditions. Most of the ultracalcic melts are intermediate between common basalts and our extreme bulk compositions. They could have formation conditions intermediate between the extremes and typical basalt-forming temperatures and pressures or may be viewed as mixtures between extreme ultracalcic and basaltic melts (e.g., Schiano et al. 2000).

Origin of the hypersthene-normative ultracalcic melts

There are two distinct ways for generating high CaO/Al_2O_3 melts: melting of CaO-rich (cpx-rich) sources at high melt fractions (Kogiso and Hirschmann 2001, Schwab and Johnston 2001) or melting of refractory clinopyroxene-poor sources at low melt fractions (Kogiso and Hirschmann 2001; Schmidt et al. 2004). Clinopyroxene assimilation has been proposed for ultracalcic hypersthene-normative lavas (the Vanuatu "ankaramites" of Schmidt et al. 2004), however this requires unrealistic amounts of assimilant (Barsdell and Berry 1990). Two hypotheses for the origin of hypersthene-normative ultracalcic melts have thus to be discussed: first, the investigated composition CaHy represents the parental magma of the hypersthene-normative suite and these magmas origin from an olivine + clinopyroxene dominant source leaving a wehrlitic residue, or second, the composition CaHy is already fractionated and the parental melt originates from a mantle composition (lherzolite or clinopyroxene-bearing harzburgite) at even higher temperatures.

The liquidus phases of the hypersthene-normative composition CaHy suggest an olivine + clinopyroxene residue at 1.2 GPa, 1,410°C. Melting of olivine + clinopyroxene—dominant starting materials has been investigated by Kogiso and Hirschmann (2001; OlCpx1) and Schwab and Johnston (2001; INT-B), the later starting material containing 7 wt% orthopyroxene. As for lherzolite melting, CaO/Al_2O_3 ratios and CaO contents of partial melts were found to increase strongly with melt fraction (at 1.0 GPa, Fig. 6). However, the studied wehrlitic compositions are more clinopyroxene-rich than a lherzolite and clinopyroxenes are more Ca-rich, such that higher CaO contents and higher CaO/Al_2O_3 ratios could be reached in partial melts. The experimental melts of Kogiso and Hirschmann (2001) become ultracalcic at high temperatures (≥1,350°C) and at high degrees of melting (≥30%) but remain nepheline-normative. Schwab and Johnston (2001) have obtained hypersthene-normative ultracalcic melts at similar melting temperatures (~1,360°C at 1.0 GPa) and significantly lower melt fractions (down to 12 wt%). The comparatively lower melt fractions are a consequence of a higher olivine content of Schwab and Johnston's starting material (50 wt% vs. 25 wt% in Kogiso and Hirschmann's experiments).

During clinopyroxene—melting, minor pyroxene components hypersthene, jadeite, and Ca-Tschermaks will be concentrated in the liquid phase relative to a residual diopside-rich clinopyroxene, as shown by experimental phase relations for clinopyroxene binary systems (diopside-CaTschermack: Schairer and Yoder 1969; diopside-jadeite: Bell and Davis 1969; diopside-hypersthene: Kushiro 1969). The strong partitioning of these components into melts at the lowest experimental temperatures controls the nepheline- or hypersthene-normative character of the first partial melts that form. For Schwab and Johnston's (2001) experiments, the hypersthene-normative character of the melts (Fig. 7) is

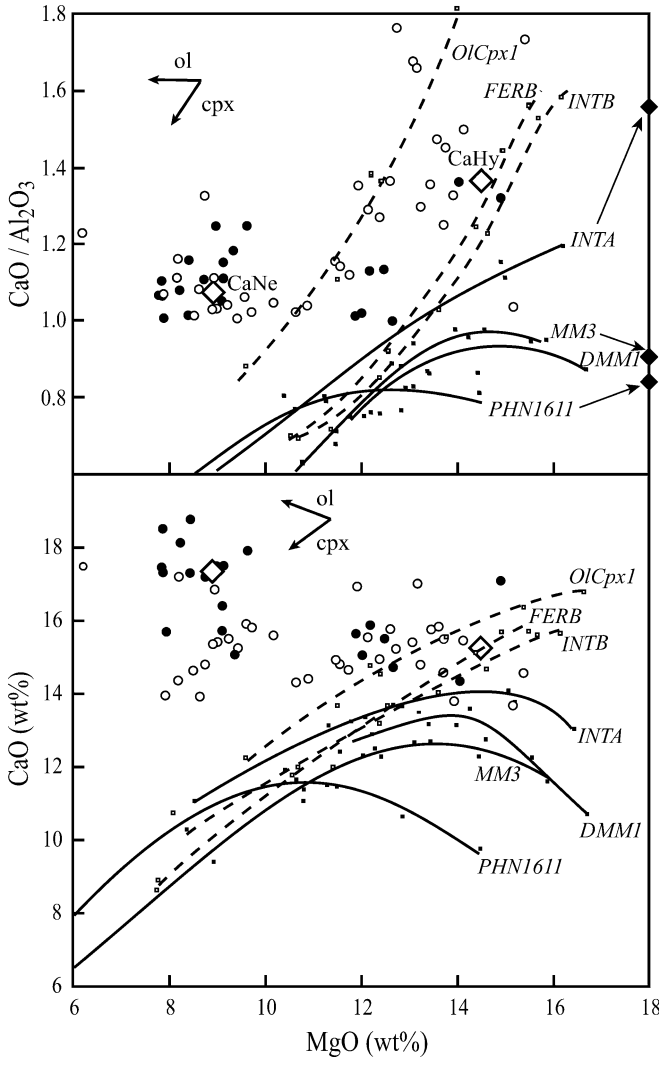

Fig. 6 CaO vs. MgO and CaO/Al_2O_3 vs. MgO plots showing the evolution of experimental partial melts from lherzolites (■ ——) and wehrlites (□ - - - - - -), together with hypersthene-normative ultracalcic melt inclusions and whole rocks (*open circle*) and nepheline-normative ultracalcic melt inclusions and whole rocks (*filled circle*). Experimental melting trends at 1.0 GPa are from Baker and Stolper (1994) corrected by Hirschmann et al. (1998)-MM3, Kushiro (1996)-PHN1611, Pickering-Witter and Johnston (2000)-FERB, Schwab and Johnston (2001)-INTA and INTB, Kogiso and Hirschmann (2001)-OlCpx1, and Wasylenki et al. (2003)-DMM1. Bulk CaO/Al_2O_3 of the lherzolites are plotted to the *right* of the diagram; bulk CaO/Al_2O_3 of the wehrlites are out of scale (1.7 for FERB, 3.1 for OlCpx1, 3.4 for INTB)

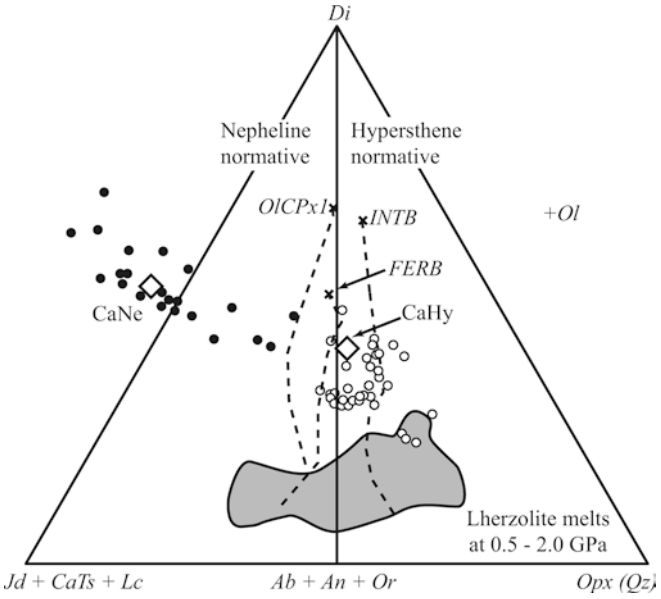

Fig. 7 Ternary diagram comparing data for ultracalcic inclusions and whole-rocks with liquids produced by melting experiments on olivine + clinopyroxene rich rocks. Molecular normative projection from Ol onto the Di-Qz-Jd + CaTs + Lc face of the "basalt tetrahedron", after Falloon and Green (1988). Same symbols as Fig. 6. Experimental melting trends of olivine + clinopyroxene-dominant rocks at 1.0 GPa are from: Kogiso and Hirschmann (2001-OlCpx1), Pickering-Witter and Johnston (2000-FERB) and Schwab and Johnston (2001-FERB). Source composition controls the hypersthene- or nepheline- normative character of the partial melts

due to initially 7 wt% of orthopyroxene in INT-B starting material. Kogiso and Hirschmann (2001) obtained slightly nepheline-normative ultracalcic melts (Fig. 7) from a slightly nepheline-normative starting material (jadeite + CaTschermak enriched; 0.84 wt% Na_2O and 5.58 wt% Al_2O_3). With increasing temperature, melt compositions then follow an olivine-clinopyroxene cotectic and become ultracalcic along this cotectic.

An alternative to a wehrlitic source is possible, if the CaHy composition is not a primary but a derivative melt. In this case, previous olivine fractionation may have shifted the melt composition away from the olivine + two pyroxenes saturation surface, as suggested by Schmidt et al. (2004). If CaHy is a derivative melt, multiple saturation of the parental magma of this hypersthene-normative ultracalcic melt would then occur at even higher temperatures and pressures (e.g., Falloon et al. 1999) than for CaHy (1,410°C1.2 GPa). Hirschmann et al. (1999) have shown that high CaO/Al_2O_3 ratios characterise alkali-poor, refractory peridotite sources. Schwab and Johnston (2001) have reported a maximum CaO content of 13.9 wt% (at a CaO/Al_2O_3 ratio of 1.15) produced by melting of a depleted model lherzolite (INT-A) at clinopyroxene exhaustion (1.0 GPa). Such a CaO content and CaO/Al_2O_3 ratio is still lower than the ultracalcic compositions investigated here. Schmidt et al. (2004) demonstrated that melting of a depleted, almost refractory lherzolite with a high initial CaO/Al_2O_3 ratio results in melts with CaO/Al_2O_3 ratios up to 1.57 just at clinopyroxene exhaustion. The latter result was achieved in the presence of a mixed CO_2–H_2O volatile component; at dry conditions a CaO/Al_2O_3 of 1.48 was reached at 1,400°C. In Schmidt et al. (2004), calculated melt fractions are low, in the range 4–12 wt%.

The above melting studies result in a picture coherent with the conditions of and phase compositions at the multiple saturation point. Independent of the source

composition selected, all of the above studies are based on starting materials with high bulk CaO/Al_2O_3, make use of refractory clinopyroxene compositions, and need temperatures in excess of 1,350°C in order to maintain hypersthene-normative ultracalcic melts in the liquid state. Whether the source of the hypersthene-normative melts was olivine + clinopyroxene rich and contained orthopyroxene only at melt fractions smaller than at the time of segregation of CaHy (in which case CaHy would be an unfractionated melt), or whether the source was a depleted lherzolite (in which case CaHy would have fractionated olivine) cannot be decided.

The high melting temperatures necessary for the formation of ultracalcic melts from bulk compositions dominated by olivine + refractory pyroxenes (> 1,350°C and up to > 1400°C in order to reach the highest CaO/Al_2O_3 of natural ultracalcic melts: Schwab and Johnston 2001, Kogiso and Hirschmann 2001; Schmidt et al. 2004) are in agreement with the temperature obtained for the CaHy multiple saturation point. These temperatures are significantly higher than those argued to prevail beneath mid-ocean ridges (i.e. typically 1,300°C, McKenzie and Bickle 1988). Thus, ultracalcic, hypersthene-normative compositions that have been identified at mid-ocean ridges in association with refractory residual harzburgite (e.g., Kamenetsky et al. 1998) are indicative of more elevated temperatures in the mantle (either localised or in the entire mid-ocean ridge melting regime, see Maclenan et al. 2001; Green et al. 2001). This finding is supported by the occurrence of hypersthene-normative ultracalcic melts in basalts or picrites from Iceland (Sigurdsson et al. 2000; Slater et al. 2001), where the oceanic ridge is associated with a hotspot thus generating higher mantle melting temperatures (Maclenan et al. 2001). As an alternative, the extreme temperatures might be somewhat moderated in some cases when volatiles were present during melting. Significant H_2O contents have been measured in ultracalcic melt inclusions from the Lau back-arc basin (up to 2.4 wt%, Kamenetsky et al. 1997), however, high H_2O-contents have not been observed at mid-ocean ridges (Sobolev and Chaussidon 1996).

Finally, it should be noted that melting of lherzolitic mantle at 5–7 GPa could result in high CaO/Al_2O_3 ratios (up to 1.7, Walter 1998); however the CaO content of such melts are low (~9 wt%) and require unrealistic amounts of olivine fractionation (> 30%) to increase CaO-contents to values > 13.5 wt%. Furthermore, at such high pressures, garnet is a residual phase, and would generate a characteristic trace element signature that is not observed in ultracalcic hypersthene-normative magmas (e.g., Kamenetsky et al. 1998).

Origin of the nepheline-normative ultracalcic melts

The experiments on the nepheline-normative composition indicate olivine + clinopyroxene-saturation at very low pressures (~0.2 GPa) and, compared to the hypersthene-normative melts, at low temperatures (1,220°C). Such low pressures, corresponding to 6 km depth, are quite intriguing, and we thus tested the effect of previous olivine fractionation (or incomplete correction of olivine crystallisation for the olivine-hosted melt inclusions). Olivine addition results in a moderate increase in pressure (0.12 GPa per 1 wt% olivine added) and temperature (approximately 20°C per 1 wt% olivine added, see Fig. 5) of the multiple saturation point. Within realistic bounds of olivine addition (a few percent), the low pressures of the multiple saturation point are maintained and strongly suggest an origin of nepheline-normative ultracalcic liquids within the arc crust, leaving an olivine + clinopyroxene residual mineralogy.

Nepheline normative ultracalcic magmas from arc settings are alkali-enriched and their equilibrium clinopyroxenes are more calcic (i.e., melts further from orthopyroxene saturation) than those from hypersthene-normative ultracalcic magmas. The alkaline-rich character of nepheline-normative ultracalcic melts requires a significant amount of alkalis in the source and excludes a refractory source rock such as depleted lherzolite or wehrlite. The high alkali contents in the liquid could result from low degree melting of an alkali-depleted source, however, at low pressures, low degree melting is inconsistent with high CaO/Al_2O_3 ratios (e.g. Baker and Stolper 1994; Kogiso and Hirschmann 2001). The relatively low SiO_2-contents of nepheline-normative ultracalcic liquids exclude addition of alkalis to a lherzolitic/harzburgitic source by a sub-arc fluid or silicic melt. A lherzolitic source modified by carbonatitic liquids could generate nepheline-normative melts with high CaO and low SiO_2 content, and very-high CaO/Al_2O_3 ratios up to 2.0 (Hirose 1997). However, as discussed by Schiano et al. (2000), ultracalcic nepheline-normative melt inclusions and whole-rocks do not display the trace-element signature characteristic for the involvement of carbonatitic melts.

The liquidus phases of the nepheline-normative ultracalcic liquids, i.e. olivine and clinopyroxene (compositions CaNe, CaNe + 2.5, CaNe + 5), have Mg# within, but at the lower end of the compositional range for mantle phases. The residuum left behind after extraction of CaNe from the source is represented by a mixture of the experimentally obtained clinopyroxene and olivine (Table 1). Possible source compositions are constrained to a plane defined by CaNe, and its liquidus olivine and clinopyroxene (Fig. 8). Kogiso and Hirschmann (2001) have investigated melting of a bi-mineralic wehrlite (OlCpx1, Fig. 8a), the clinopyroxene containing 0.84 wt% Na_2O and 5.58 wt% Al_2O_3. The resulting partial melts are slightly nepheline-normative, but less than the nepheline-normative ultracalcic melt array defined by melt inclusions and whole rocks (Fig. 7). In order to produce melts close to the SiO_2-poor end of this array, the source must contain at least one additional mineral, which has a low silica content, and contain significant amounts of alkalis and alumina (to obtain the nepheline-normative signature). Furthermore, this

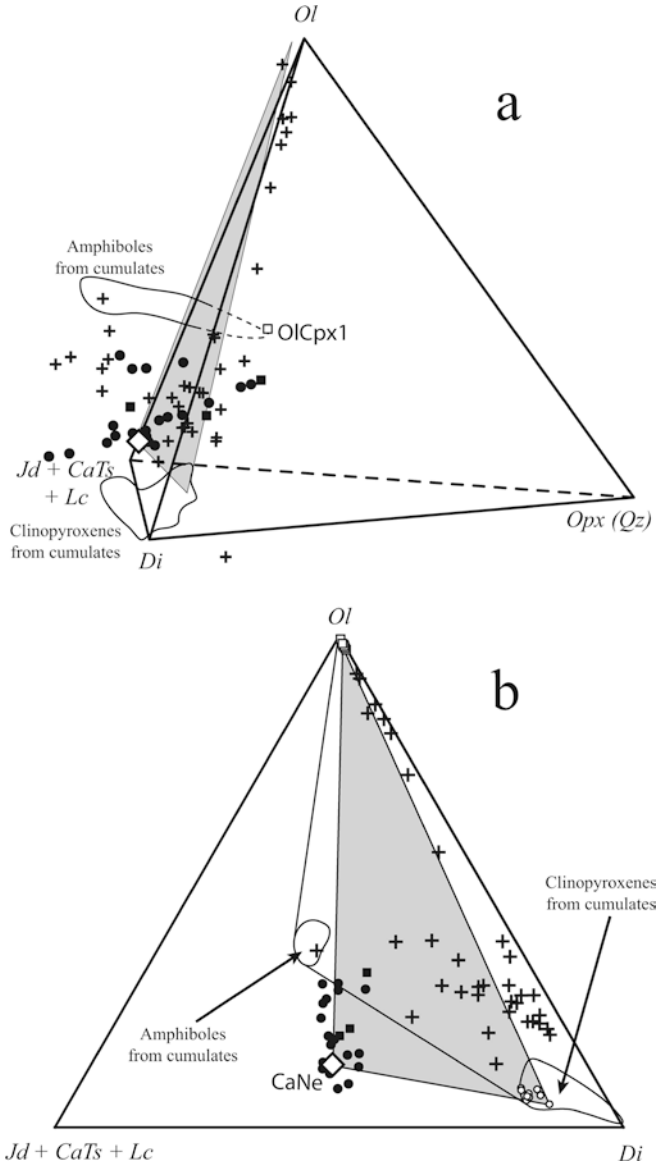

Fig. 8a, b Comparison between nepheline-normative ultracalcic liquids from arc settings (*filled circle*) and potential source compositions. **a** 3D-molecular plot into the "basalt tetrahedron", after Falloon and Green (1988). Source compositions are constrained to a surface (*grey triangle*) defined by liquidus olivine (*open square*), liquidus clinopyroxene (*open circle*), and CaNe (*open diamond*). Whole rock (+) and mineral composition of arc cumulates from Aoki (1971), Richard (1986), Debari et al. (1987), Himmelberg and Loney (1995), Turner et al. (2003). OlCpx1 is Kogiso and Hirschmann's (2001) starting composition. **b** Same data visualised on the Ol-Di-Jd + CaTs + Lc face of the "basalt tetrahedron", in projection from the SiO_2 apex. As can be seen, nepheline normative melts can be produced from a reaction in the amphibole cumulate of the type amph + cpx = ol + melt

mineral should disappear from the residue at or below 1,220°C.

Amphibole (Fig. 8) appears as an ideal candidate as it satisfies all of the aforementioned requirements and because clinopyroxene-olivine-amphibole cumulates are widely observed in arc settings, e.g. in Alaskan-type ultramafic-mafic complexes (Himmelberg and Loney 1995) or as xenoliths in basaltic arc lavas (e.g., Richard 1986). These cumulates are thought to originate from the differentiation of magnesian hydrous basalts (Himmelberg and Loney 1995), and are probably ubiquitous at the base of the arc crust (Kay and Kay 1985). Kushiro (1990) even estimated that such cumulates should build up to 50% of the crust in intraoceanic island arcs. Mg# of nepheline-normative ultracalcic melts (≤ 69.1 for melt inclusions, ≤ 73.1 for whole rocks) are lower or at the lower end of partial melts from lherzolites (e.g., Mg# 71.2–79.1, Baker and Stolper 1994), which is coherent with an origin of nepheline-normative ultracalcic magmas from cumulates of lherzolite melts. Amphibole in the source lowers melting temperatures required for generating ultracalcic melts, as pargasitic amphibole melts near 1,100°C at 1.0 GPa (Holloway 1972). If amphibole was present in the source of nepheline-normative ultracalcic magmas, then the magma itself would contain small amounts of H_2O. The presence of water slightly lowers the liquidus temperatures compared to anhydrous liquidus temperatures determined for CaNe (CaNe + 2.5, CaNe + 5), which are in the range 1,220–1,275°C. Such temperatures are readily achievable in arc settings and are in agreement with homogenisation temperatures obtained for ultracalcic nepheline-normative melt inclusions found in arcs (1,220 ± 20°C, Schiano et al. 2000). Note that a key role for amphibole has already been proposed by Della-Pasqua et al. (1995) for the origin of Al-rich melt inclusions in arc settings.

Thus, we propose that nepheline-normative ultracalcic melts from arc settings are generated upon heating of olivine-clinopyroxene-amphibole cumulates in the arc crust. Advection of hot basaltic or picritic primitive magma could heat such cumulates to the required temperatures. The ultracalcic, nepheline-normative signature would thus not be caused by a peculiar melting process but simply reflect the source composition.

Summary and conclusions

1. The liquidus phase relations constrain the very distinct conditions of origin of the two ultracalcic magma suites: they suggest a melting process at crustal conditions for the nepheline-normative melts, whereas mantle conditions are likely for generating the hypersthene-normative ultracalcic suite.
2. Our results in combination with melting experiments from the literature suggest that hypersthene-normative melts form through a melting process at mantle pressures from a refractory source that contains, at least initially, orthopyroxene. Whether hypersthene-normative melts are high-degree melts from an olivine + clinopyroxene rich source or low-degree melts from a depleted lherzolite (in which case CaHy would have fractionated olivine) cannot be decided. Nevertheless, the genesis of ultracalcic hypersthene-normative liquids requires particularly high temperatures (at least, 1,350–1,400°C), significantly above the

mantle adiabat as proposed by McKenzie and Bickle (1988) and much more in the range proposed by Green et al. (2001).

3. The alkali-rich, silica-poor nepheline-normative population instead forms at crustal pressures from olivine-clinopyroxene cumulates which must have contained some amphibole. 1,200–1,250°C are sufficient to form nepheline-normative ultracalcic melts, because of the amphibole in the source, and are compatible with temperatures that can be achieved by heating of crustal cumulates by picritic melts intruding into or accumulated at the base of the arc crust.
4. In both cases, the high CaO/Al_2O_3 signature should be inherited from the source. Following this hypothesis, the genesis of ultracalcic primitive liquids would require sources with high CaO/Al_2O_3 ratios. Their occurrence as whole rocks or as primitive melt inclusions in mid-ocean ridges and island arc basalts would trace the existence of high-CaO/Al_2O_3 rocks, either as source heterogeneities or as wall-rocks encountered by the magmas en route to the surface.

Acknowledgements This study has benefited from discussions with D. Laporte, E.M. Stolper and P. Boivin. We thank A. Provost for his mass-balance program and M. Veschambre for technical assistance with the electron probe microanalysis. The manuscript has been improved by constructive reviews by D.H. Green and M.M. Hirschmann. Financial support was provided by the European Community's Human Potential Programme under contract HPRN-CT-2002–00211 (Euromelt) and by INSU-CNRS (I.T. programme).

References

Albarède F, Provost A (1977) Petrologic and geochemical mass-balance equations: an algorithm for least-square fitting and general error analysis. Comput Geosci 3:309–326

Ancey M, Bastenaire F, Tixier R (1978) Application des méthodes statistiques en microanalyse. In: Maurice F, Meny L, Tixier R (eds) Microanalyse, microscopie électronique à balayage. Les Editions du Physicien, Orsay, pp 323–347

Aoki KI (1971) Petrology of mafic inclusions from Itinome-gata, Japan. Contrib Miner Petrol 30:314–331

Baker MB, Stolper EM (1994) Determining the composition of high-pressure mantle melts using diamond aggregates. Geochim Cosmochim Acta 58:2811–2827

Barsdell M, Berry RF (1990) Origin and evolution of primitive island arc ankaramites from Western Epi, Vanuatu. J Petrol 31:747–777

Basaltic Volcanism Study Project (1981) Basaltic Volcanism on the Terrestrial Planets. Pergamon Press, Inc., New York, p 1286

Bell PM, Davis BTC (1969) Melting relations in the system jadeite-diopside at 30 and 40 kilobars. Am J Sci 267-A:17–32

Brey G, Green DH (1977) Systematic study of liquidus phase relations in olivine melilitite + H_2O + CO_2 at high pressures and petrogenesis of an olivine melilitite magma. Contrib Miner Petrol 61:141–162

Brey G, Huth J (1984) The enstatite-diopside solvus to 60 kbar. In: Kornprobst J (ed) Kimberlites II: the mantle and crust-mantle relationships. Elsevier, Amsterdam pp 257–264

De Hoog JCM, Mason PRD, van Bergen MJ (2001) Sulfur and chalcophile elements in subduction zones: constraints from a laser ablation ICP-MS study of melt inclusions from Galunggung Volcano, Indonesia. Geochim Cosmochim Acta 65:3147–3164

Debari S, Kay SM, Kay RW (1987) Ultramafic xenoliths from Adagdak volcano, Adak, Aleutian Islands, Alaska: deformed igneous cumulates from the MOHO of an island arc. J Geol 95:329–341

Della-Pasqua FN, Varne R (1997) Primitive ankaramitic magmas in volcanic arcs: a melt-inclusion approach. Can Miner 35:291–312

Della-Pasqua FN, Kamenetsky VS, Gasparon M, Crawford AJ, Varne R (1995) Al-spinels in primitive arc volcanics. Miner Petrol 53:1–26

Dunworth EA, Wilson M (1998) Olivine melilitites of the SW German tertiary volcanic province: mineralogy and petrogenesis. J Petrol 39:1805–1836

Falloon TJ, Green DH (1988) Anhydrous partial melting of peridotite from 8 to 35 kb and the petrogenesis of MORB. J Petrol Spec Lithosphere Issue, pp 379–414

Falloon TJ, Green DH, Jacques AL, Hawkins JW (1999) Refractory magmas in back-arc basin settings—experimental constraints on the petrogenesis of a Lau Basin example. J Petrol 40:255–277

Gaetani GA, Cherniak DJ, Watson EB (2002) Diffusive reequilibration of CaO in olivine-hosted melt inclusions. In: Goldschmidt Conference Abstracts, p A254

Gerlach TM, Graeber EJ (1985) Volatile budget of Kilauea volcano. Nature 313:273–277

Green DH, Falloon TJ, Eggins SM, Yaxley GM (2001) Primary magmas and mantle temperatures. Eur J Miner 13:437–451

Green DH, Schmidt MW, Hibberson, WO (2004) Island-arc ankaramites: primitive melts from fluxed refractory lherzolitic mantle. J Petrol 45:391–403

Gust DA, Perfit MR (1987) Phase relations of a high-Mg basalt from the Aleutian Island Arc: implications for primary island arc basalts and high-Al basalts. Contrib Miner Petrol 97:7–18

Himmelberg GR, Loney RA (1995) Characteristics and petrogenesis of Alaskan-type ultramafic-mafic intrusions, southeastern Alaska. USGS Prof Paper 1564

Hirose K (1997) Partial melt compositions of carbonated peridotite at 3 GPa and role of CO_2 in the alkali-basalt magma generation. Geophys Res Lett 24:2837–2840

Hirose K, Kawamoto T (1995) Hydrous partial melting of lherzolite at 1 GPa: the effect of H_2O on the genesis of basaltic magmas. Earth Planet Sci Lett 133:463–473

Hirose K, Kushiro I (1993) Partial melting of dry peridotites at high pressures: determination of compositions of melts segregated from peridotites using aggregates of diamonds. Earth Planet Sci Lett 114:477–489

Hirschmann MM, Stolper EM (1996) A possible role for garnet pyroxenite in the origin of the "garnet signature" in MORB. Contrib Miner Petrol 124:185–208

Hirschmann MM, Baker MB, Stolper EM (1998) The effect of alkalis on the silica content of mantle-derived melts. Geochim Cosmochim Acta 62:883–902

Hirschmann MM, Ghiorso MS, Stolper EM (1999) Calculation of peridotite partial melting from thermodynamic models of minerals and melts. II. Isobaric variations in melts near the solidus and owing to variable source composition. J Petrol 40:297–313

Holloway JR (1972) The system pargasite-H_2O–CO_2: a model for melting of a hydrous mineral with a mixed-volatile fluid—I. Experimental results to 8 kbar. Geochim Cosmochim Acta 37:351–666

Holloway JR, Pan V, Gudmundsson G (1992) High-pressure fluid-absent melting experiments in the presence of graphite: oxygen fugacity, ferric/ferrous ratio and dissolved CO_2. Eur J Miner 4:105–114

Jambon A (1994) Earth degassing and large-scale geochemical cycling of volatile elements. In: Carroll MR, Holloway JR (eds) Volatiles in magmas, Reviews in Mineralogy 30. Mineralogical Society of America, pp 479–517

Jaques AL, Green DH (1980) Anhydrous melting of peridotite at 0–15 kb pressure and the genesis of tholeiitic basalts. Contrib Miner Petrol 73:287–310

Kamenetsky VS, Crawford AJ, Eggins S, Mühe R (1997) Phenocryst and melt inclusion chemistry of near-axis seamounts, Valu Fa Ridge, Lau Basin: insight into mantle wedge melting and the addition of subduction components. Earth Planet Sci Lett 151:205–223

Kamenetsky VS, Eggins SM, Crawford AJ, Green DH, Gasparon M, Falloon TJ (1998) Calcic melt inclusions in primitive olivine at 43°N MAR: evidence for melt-rock reaction/melting involving clinopyroxene-rich lithologies during MORB generation. Earth Planet Sci Lett 160:115–132

Kay SM, Kay RW (1985) Role of crystal cumulates and the oceanic crust in the formation of the lower crust of the Aleutian arc. Geology 13:461–464

Kogiso T, Hirschmann MM (2001) Experimental study of clinopyroxenite partial melting and the origin of ultra-calcic melt inclusions. Contrib Miner Petrol 142:347–360

Kushiro I (1969) The system forsterite-diopside-silica with and without water at high pressures. Am J Sci 267A:269–294

Kushiro I (1990) Partial melting of mantle wedge and evolution of island arc crust. J Geophys Res 95:15929–15939

Kushiro I (1996) Partial melting of a fertile mantle peridotite at high pressures: an experimental study using aggregates of diamond. In: Earth processes: reading the isotopic code. Geophys Monogr 95:109–102

Laporte D, Toplis M, Seyler M, Devidal J-L (2004) A new experimental technique for extracting liquids from peridotite at very low degrees of melting: application to partial melting of depleted peridotite. Contrib Miner Petrol 146:463–484

Libourel G (1999) Systematics of calcium partitioning between olivine and silicate melt: implications for melt structure and calcium content of magmatic olivine. Contrib Miner Petrol 136:63–80

Maclenan J, McKenzie D, Grönvold K (2001) Plume-driven upwelling under central Iceland. Earth Planet Sci Lett 194:67–82

McKenzie D, Bickle MJ (1988) The volume and composition of melt generated by extension of the lithosphere. J Petrol 29:625–679

O'Neill (1987) Quartz-fayalite-iron and quartz-fayalite-magnetite equilibria and the free energy of formation of fayalite (Fe_2SiO_4) and magnetite (Fe_3O_4). Am Miner 72:67–75

O'Neill HSC, Pownceby MI (1993) Thermodynamic data from redox reactions at high temperatures. I. An experimental and theoretical assessment of the electrochemical method using stabilized zirconia electrolytes, with revised values for the Fe–"FeO", Co–CoO, Ni–NiO and Cu–Cu_2O oxygen buffers, and new data for the W-WO_2 buffer. Contrib Miner Petrol 114:296–314

Pertermann M, Hirschmann MM (2003) Partial melting experiments on a MORB-like pyroxenite between 2 and 3 GPa: constraints on the presence of pyroxenite in basalt source regions from solidus location and melting rate. J Geophys Res 108:2125. DOI 10.1029/2000JB000118

Pichavant M, Mysen BO, Macdonald R (2002) Source and H_2O content of high-MgO magmas in island arc settings: an experimental study of a primitive calc-alkaline basalt from St. Vincent, Lesser Antilles arc. Geochim Cosmochim Acta 66:2193–2209

Pickering-Witter J, Johnston AD (2000) The effects of variable bulk composition on the melting systematic of fertile peridotitic assemblages. Contrib Miner Petrol 140:190–211

Richard M (1986) Géologie et Pétrologie d'un jalon de l'arc Taïwan-Luzon : l'île de Batan (Philippines). PhD Thesis, Université de Bretagne Occidentale

Schairer JF, Yoder HS (1969) Critical planes and flow and flow sheet for a portion of the system CaO–MgO–Al_2O_3–SiO_2 having petrological implications. Carnegie Inst. Washington. Ann Rept Dir Geophys Lab, pp 202–214

Schiano P, Eiler JM, Hutcheon ID, Stolper EM (2000) Primitive CaO-rich, silica-undersaturated melts in island arcs: evidence for the involvement of clinopyroxene-rich lithologies in the petrogenesis of arc magmas. Geochem Geophys Geosys 1:1999GC000032

Schmidt MW, Green DH, Hibberson WO (2004) Ultracalcic magmas generated from Ca-depleted mantle: an experimental study on the origin of ankaramites. J Petrol 45:531–554

Schwab BE, Johnston AD (2001) Melting systematics of modally variable, compositionally intermediate peridotites and the effects of mineral fertility. J Petrol 42:1789–1811

Sigurdsson IA, Steinthorsson S, Grönvold K (2000) Calcium-rich melt inclusions in Cr-spinels from Borgarhraun, northern Iceland. Earth Planet Sci Lett 183:15–26

Slater L, McKenzie D, Grönvold K, Shimizu N (2001) Melt migration and movement beneath Theistareykir, NE Iceland. J Petrol 42:321–354

Sobolev AV, Chaussidon M (1996) H_2O concentrations in primary melts from supra-subduction zones and mid-ocean ridges: implications for H_2O storage and recycling in the mantle. Earth Planet Sci Lett 137:45–55

Soulard H, Provost A, Boivin P (1992) CaO–MgO–Al_2O_3–SiO_2–Na_2O (CMASN) at 1 bar from low to high Na_2O contents; topology of an analogue for alkaline basic rocks. Chem Geol 96:459–477

Thibault Y, Holloway JR (1994) Solubility of CO_2 in a Ca-rich leucitite: effects of pressure, temperature, and oxygen fugacity. Contrib Miner Petrol 116:216–224

Trønnes RG (1990) Basaltic melt evolution of the Hengill volcanic system, SW Iceland, and evidence for clinopyroxene assimilation in primitive tholeiitic magmas. J Geophys Res 95:15893–15910

Turner S, Foden J, George R, Evans P, Varne R, Elburg M, Jenner G (2003) Rates and processes of potassic magma evolution beneath Sangeang Api volcano, East Sunda arc, Indonesia. J Petrol 44:491–515

Ulmer P (1989) The dependence of the Fe2+-Mg cation-partitioning between olivine and basaltic liquid on pressure, temperature and composition; an experimental study to 30 kbars. Contrib Miner Petrol 101:261–273

Vielzeuf D, Clemens J (1992) The fluid-absent melting of phlogopite + quartz; experiments and models. Am Miner 77:1206–1222

Walter MJ (1998) Melting of garnet peridotite and the origin of komatiite and depleted lithosphere. J Petrol 39:29–60

Wasylenki LE, Baker MB, Kent AJR, Stolper EM (2003) Near-solidus melting of the shallow upper mantle: partial melting experiments on depleted peridotite. J Petrol 44:1163–1191